Journal of Non-Crystalline Solids 617 (2023) 122505

Contents lists available at ScienceDirect

Journal of Non-Crystalline Solids

journal homepage: www.elsevier.com/locate/jnoncrysol

Exploring the dielectric polarization and ionic conduction mechanisms in sodium-containing silicate and borosilicate glasses

Cesar A. Nieves [a,b,*], Michael T. Lanagan [b,c]

[a] Department of Materials Science and Engineering, The Pennsylvania State University, University Park, PA 16802, United States of America
[b] Materials Research Institute, The Pennsylvania State University, University Park, PA 16802, United States of America
[c] Department of Engineering Science and Mechanics, The Pennsylvania State University, University Park, PA 16802, United States of America

ARTICLE INFO

Keywords:
Glass
Sodium migration
Ionic conduction
Relaxation processes
Thermal poling
Activation energy

ABSTRACT

The dielectric and electrical behavior of a sodium silicate glass (soda-lime-silica; SLS) and a sodium borosilicate glass (D263T) are systematically and comprehensively characterized by a combination of ac and dc techniques at various temperatures and electric fields. This study reveals that Na^+ migration primarily influences the dielectric loss, energy efficiency, and leakage current in these glasses, with a less detrimental effect in D263T due to its higher activation energy for ionic conduction. Moreover, this study identifies an additional relaxation mechanism contributing to the leakage current in D263T which was not observed in SLS. The origin of this mechanism has not been extensively explored, and it is believed to arise from a more limited migration of Na^+ ions associated with the short migration and accumulation of a second and less mobile ion near the anode.

1. Introduction

New technologies for reducing CO_2 emissions have received increased attention in the transportation and energy sector in recent years. Electric vehicles and solar energy are promising renewable and sustainable technologies that can get us closer to achieving a cleaner world. As we attempt to make that possible and meet the evolving demands of these sectors, researchers and manufacturers continue to develop new dielectric materials that exhibit low electrical conductivity, low dielectric loss, high optical transparency, chemical durability, mechanical stability, and cost-efficient production. Glass is an excellent candidate as a dielectric material due to its tremendous versatility and technical capabilities [1]. For example, silica glass or vitreous silica (SiO_2) is generally used in applications where low electrical conductivity, extremely high operating temperatures, high transparency, and very low coefficient of thermal expansion (CTE) are required (e.g., optical fibers and astronomical mirrors). However, its usage is limited by its high manufacturing cost [2].

Alkali oxides (e.g., Na_2O and K_2O) and alkaline earth oxides (e.g., CaO and BaO) are commonly introduced to the glass network structure as network modifiers (NWM) to tailor-engineer the glass composition and structure. The addition of NWM is a key factor in decreasing manufacturing costs and tailoring the glass properties as needed, thus offering solutions to many applications. For instance, alkali oxides (e.g., Na_2O) are usually used to reduce the glass melting temperature while alkaline earth oxides (e.g., CaO) are added to stabilize the glass network, thus improving chemical durability. However, the addition of NMWs strongly influences the electrical properties and dielectric properties of the glass [3,4]. When NWM is added to the SiO_2 network structure, it disrupts the continuous network structure of SiO_2 by breaking the silicate backbone (Si–O–Si) by forming nonbridging oxygens (NBO; Si–O^-), changing the network speciation and decreasing the connectivity of the glass [5]. In borosilicate (B_2O_3·SiO_2) glass, the addition of NWM induces the conversion of the three-fold coordinated boron (BO_3 trigonal or B^{III}) to four-coordinated boron ($[BO_4]^-$ tetrahedra) with little or none NBOs formation [6–10]. In both glasses, the NMW as a cation (e.g., Na^+, Ka^+, Ca^{2+}, Ba^{2+}), occupies the voids in the silica framework and charge compensates for the negatively charged NBO and $[BO_4]^-$ tetrahedra (or B^{IV}), for the silicate and borosilicate glass, respectively. This structural modification creates mobile ions which allow the movement of charges within the glass structure, affecting the ionic conductivity and dielectric polarizability, and ultimately the dielectric permittivity and dielectric loss of the glass [3,4,11–13].

When glass is subjected to electric field conditions, highly mobile ions such as Na^+ produce dielectric polarization at high frequencies by reorienting locally via local hopping. They are also responsible for the

* Corresponding author.
E-mail address: can34@psu.edu (C.A. Nieves).

https://doi.org/10.1016/j.jnoncrysol.2023.122505
Received 6 June 2023; Received in revised form 13 July 2023; Accepted 14 July 2023
Available online 24 July 2023

electrical conduction in lower frequencies by separating themselves from their immediate neighborhood NBO or $[BO_4]^-$ tetrahedra. The long-range motion of Na^+ ions is also responsible for many reliability issues in many applications. For example, the migration of Na^+ ions from the front cover glass to the solar cell in photovoltaic modules results in efficiency loss and reduce glass transparency [14,15]. Temperature also plays a crucial factor in this phenomenon since elevated temperatures can accelerate the migration of Na^+ ions, intensifying the detrimental effects on the overall performance.

This work aimed to investigate the influence of mobile ions on the dielectric and electrical properties of two types of glasses: sodium silicate glass (soda-lime-silica; SLS) and sodium borosilicate glass (D263T). To achieve this, a comprehensive set of ac and dc measurement techniques was employed with a particular emphasis on elevated temperatures where the influence of mobile ions becomes more pronounced. Particularly, we present electrochemical impedance spectroscopy (EIS), dielectric displacement-electric field (D-E) loops, and thermally stimulated depolarization current (TSDC) measurements under varying temperatures and electric field conditions. Through this multidimensional analysis, we aimed to gain a thorough understanding of how the composition and structure of these glasses influence their dielectric and electrical characteristics.

2. Experimental procedure

2.1. Sample preparation

In this study, we used soda-lime-silica (SLS) float glass (AGC, Japan, size 25 mm x 25 mm x 0.7 mm), with a chemical composition of 71.7 wt. % SiO_2, 13.1 wt.% Na_2O, 8.13 wt.% CaO, 4.4 wt.% MgO, 1.61 wt.% Al_2O_3, and other elements in trace concentrations inherent to the Pilkington float process [16], and Schott D263T (Schott technologies Inc., size 25 mm x 25 mm x 0.1 mm) with a chemical composition of 64.1 wt. % SiO_2, 8.4 wt.% B_2O_3, 6.4 wt.% Na_2O, 6.9 wt.% K_2O, 4.2 wt.% Al_2O_3, 5.9 wt.% ZnO, and 4.0 wt.% TiO_2 [17]. Both glasses were specifically chosen due to their high Na content, which made them excellent candidates for in-depth exploration of the mechanisms of dielectric polarization and ionic conduction. Prior to experimentation, the glass samples were thoroughly cleaned via sonication in acetone and ethanol to eliminate surface contaminants.

2.2. Dielectric and electrical measurements

Electrochemical impedance spectroscopy (EIS) is a commonly used ac technique to study the mechanisms of dielectric polarization in a dielectric material. This is a powerful technique used to investigate bound and mobile charges in the bulk and interfacial regions of a dielectric material associated with the frequency of the applied ac signal. The EIS measurements were carried out in a frequency response analyzer (Solartron Analytical Modulab XM MTS) coupled to a Delta Design 9023 Environmental Test Chamber with a temperature controller. The measurements were performed by applying a small ac voltage signal of 0.5 V in the frequency range of 0.1 Hz to 100 kHz and the temperature range of 150 °C to 250 °C, in steps of 25 °C. Before each measurement, the temperature was held for 20 mins to reach a thermal quasi-steady state. Dielectric displacement-electric field (D-E) hysteresis is a complementary ac technique to characterize low- and high-field ac losses in the low-frequency regime. The D-E loops were taken under an applied ac voltage signal using a Stanford Research System model 830 DSP lock-in amplifier (Sunnyvale, CA, USA). Here, low-field D-E loops were measured between 10 and 30 V, in steps of 5 V, at a fixed frequency of 100 Hz. The high-field D-E loops were taken under an applied ac voltage signal of 600 V at 10 Hz and at 100 Hz. Both the low and high field D-E hysteresis loops were measured at room temperature (RT) and 150 °C for comparison. The D-E loops at 150 °C were carried out by immersing the glass samples in a bath of dielectric fluid (Galden HT-200; Solvay Solexis, Houston, TX) which acted as an inert medium. Both EIS and D-E loops measurements were conducted in glass samples with 50-nm aluminum upper and bottom electrodes with an electrode area of 17.67×10^{-5} m^2.

The thermally stimulated depolarization current (TSDC) method has been widely used to study the migration of ions in thermally poled silicate and multicomponent glasses [16,18–22]. Thermal poling in glass and the TSDC procedure is similar to the one described in a previous work [16], and it can be summarized as follow:

1 The glass sample is heated to a poling temperature (T_p) below the glass transition temperature of the glass.
2 Then, a dc poling voltage (V_p) is applied to the glass sample and the polarization current (I_p) or leakage current is monitored as a function of the poling time (t_p).
3 While V_p is still applied, the sample is rapidly cooled to a lower temperature using liquid nitrogen where the mobility of the ions is significantly reduced resulting in a “frozen-in” polarization state.
4 The glass sample is then short-circuited and reheated at a constant rate β of 10 °C min^{-1}. As the sample is reheated, the depolarization current (I_d) is recorded as a function of temperature.

Glass samples with 50-nm aluminum upper and guarded bottom electrodes, following the standard test method ASTM D257-14), and an effective area of 11.31×10^{-5} m^2 were used for the TSDC measurements. The TSDC measurements in this study involved subjecting the samples to successive poling conditions. The poling voltage (V_p) was varied from 20 V to 60 V in increments of 20 V, while t_p and T_p, were kept the same for all the cycles. The poling time was set to 20 min, and the poling temperature was maintained at 250 °C. After each poling cycle, the samples were cooled to 50 °C and then reheated to 250 °C at a constant rate (β) of 10 °C per minute. The depolarization current (I_d) was recorded after each cycle as the temperature increased from 50 °C to 250 °C.

3. Results and discussion

3.1. Complex impedance and ac conductivity

The real (Z') and the imaginary (Z") parts of the complex impedance for SLS and D263T for several temperatures are shown in Fig. 1(a) and (b). The data plots show the resistive and capacitive response of both glass samples as Nyquist representation. The complex impedance plot in both glass compositions exhibits an apparent semi-circle corresponding to the bulk response. At low frequencies, SLS exhibits an arc segment at all temperatures which is attributed to space-charge contributions that arise from the short-range motion and local redistribution of ionic species near the electrode surfaces (e.g., electrode polarization). D263T shows a similar response at temperatures higher than 200 °C. It is evident that the values bulk resistance (R_{bulk}) –extracted from the intersection point of the semi-circle and the x-axis at the low-frequency region where Z" is 0– are higher for D263T compared to SLS at all temperatures. The lower sodium content and the higher network connectivity are responsible for the higher R_{bulk} in D263T. Additionally, it is well known that the corresponding mobility decrease in mixed alkali systems, also known as the mixed alkali effect [23,24]. Moreover, the R_{bulk} and the overall diameter of the semi-circle decrease with temperature. The reduction of the overall impedance is the result of an increment in ionic mobility due to the nature of the conduction process which is thermally activated.

To describe the deviation from the relaxation of a single relaxation model, the variation of the normalized imaginary impedance Z"(f)/Z"$_{max}$ versus $\log_{10}[f/f_{max}]$ for several temperatures are shown in Fig. 1 (c) and (d) for SLS and D263T, respectively. The overlapping of the peak position into a master curve suggests that the dynamic process of the charge carriers does not change with temperature (i.e., similar

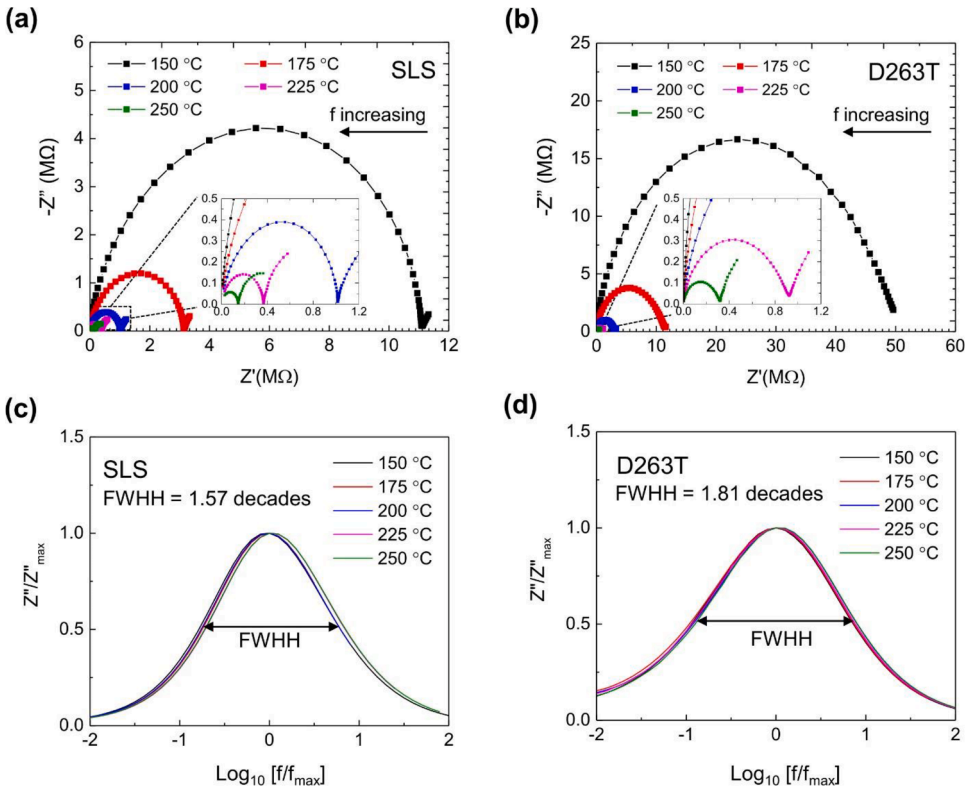

Fig. 1. (a-b) Complex impedance and (c-d) normalized Z''(f)/Z''$_{max}$ for SLS and D263T measured at several temperatures.

activation energy). A gaussian fitting of the normalized imaginary impedance gave values of the full width at half height (FWHH) of 1.57 decades for SLS and 1.81 decades for D263T (1.14 decades for an ideal Debye relaxation), which confirms that this relaxation follows a non-Debye-type behavior [25]. This deviation might be caused by a distribution of local conductivities and dielectric response times associated with inhomogeneity in the system which is experimentally represented with a constant phase element [26].

The bulk conductivity (σ_{bulk}) of the species contributing to the overall conduction can be estimated as follow:

$$\sigma_{bulk} = \frac{l}{R_{bulk} \cdot A}, \quad (1)$$

where l and A denote the thickness and the area of the glass sample, respectively. As described before, the conduction in both glasses is a thermally activated process thus, an Arrhenius relation can be implemented using Eq. (1). The temperature-dependent bulk conductivity is obtained by linearization of the expression:

$$\sigma_{bulk} = \sigma_0 \exp\left(-\frac{E_a}{k_b T}\right), \quad (2)$$

where σ_0 is the pre-exponential factor, k_b is Boltzmann's constant, T is the temperature, and E_a is the activation energy associated with the type of conduction process.

As illustrated in Fig. 2, the log σ_{bulk} vs 1000/T shows a linear response for both glasses which indicates that the conduction mechanism is independent of the temperature evaluated in this work. From the slope, the activation energy was calculated yielding values of 0.83 eV for SLS and 0.97 eV for D263T. From the main component of these glasses, Na^+ and Ca^{2+} ions in SLS and Na^+ and K^+ ions in D263T could contribute to bulk conduction. However, the higher cation field strength and larger ionic radius of Ca^{2+} and K^+ compared to Na^+, result in stronger bonding with the counterion, leading to lower mobility. Therefore, the activation energy for bulk conduction in SLS and D263T is believed to be primarily

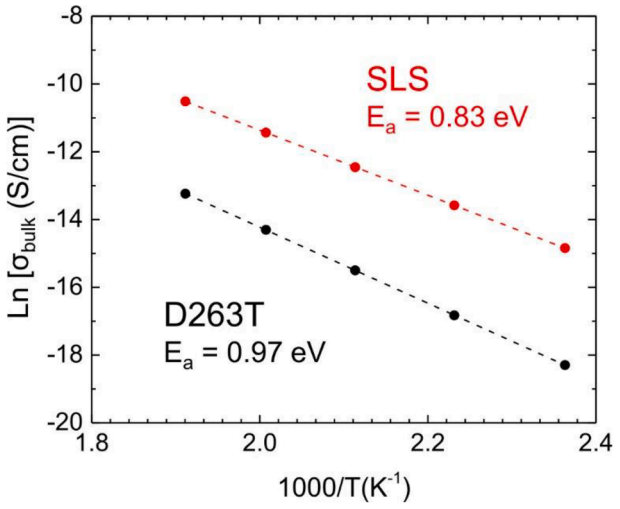

Fig. 2. Temperature-dependent bulk conductivity for SLS and D263T.

associated with the motion of Na^+ ions. These observations and activation energy values are in good agreement with values reported for several high Na-containing glasses [11,27–30].

The temperature dependence of the dielectric loss (tanδ) and the variation of ac conductivity with frequency at different temperatures for SLS and D263T are shown in Fig. 3(a) and (b), respectively. The ac conductivity values were calculated from the experimental data using the following expression:

$$\sigma_{ac} = 2\pi f \varepsilon_0 \varepsilon_r \tan\delta, \quad (4)$$

where f is the frequency of the applied ac signal, ε_0 is the permittivity of free space, and ε_r is the relative permittivity of the glass. From the tanδ, a strong loss peak is observed for both samples, characterized by a shift

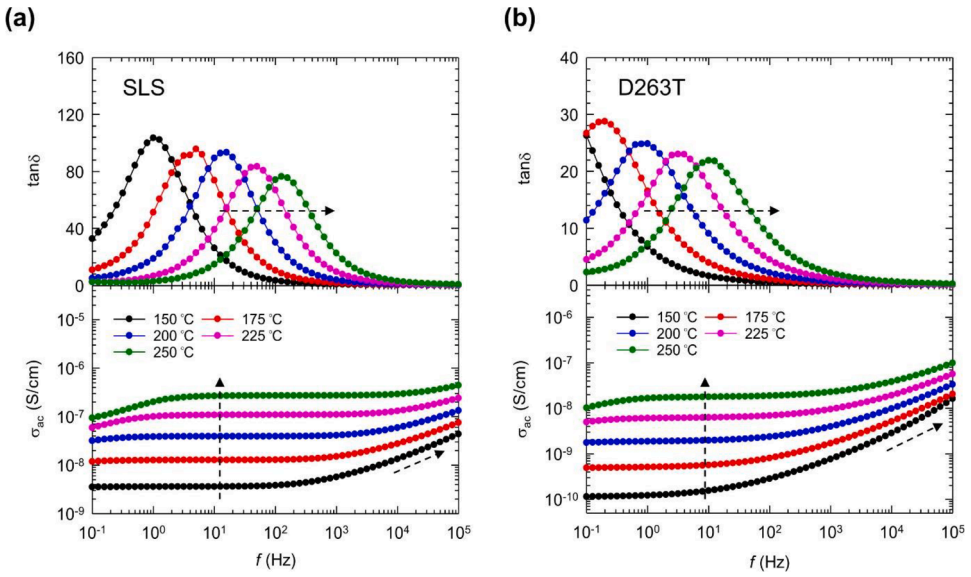

Fig. 3. Measured tanδ and ac conductivity for (a) SLS and (b) D263T for several temperatures.

towards higher frequencies and a decrease in intensity as temperature increases. The former implies a thermally activated process and the latter is attributed to a decrease in polarizability.

An Arrhenius-type relation is also implemented to calculate the activation energy due to the variation in the relaxation time τ. The relaxation time associated with the dielectric loss is estimated using the frequency where tanδ is maxima ($\tau^{\tan\delta} = 1/2\pi f_{max}$). The variation of the relaxation time $\tau^{\tan\delta}$ is plotted as a function of 1000/T, and the activation energy is calculated using the relation:

$$\tau^{tan\delta} = \tau_0 \exp\left(-\frac{E_a}{k_b T}\right), \tag{3}$$

where τ_0 is the pre-exponential factor and the other terms were as previously defined. The activation energy shown in Fig. 4(a), 0.92 eV for SLS and 1.05 eV for D263T, are slightly higher than the values of E_a estimated using Eq. (2) for bulk conductivity. This can be attributed to the fact that the bulk conductivity estimates are derived from slightly higher frequencies than those used in the calculation of relaxation time, which is determined by the frequency at which tanδ reaches its maximum. Despite this difference, the estimated values are comparable, indicating a similar origin for both processes.

Moreover, as shown in Fig 3, the ac conductivity reveals two main regions in the studied frequency range. At low frequencies, a plateau region where the ac conductivity is independent of frequency is attributed to dc conduction. It is also worth noting that at high temperatures and frequencies lower than 1 Hz, a decrement in ac conductivity is observed due to the electrode polarization, as previously discussed. At higher frequencies, a frequency dispersion region is observed, wherein the conductivity increases while the temperature dependence weakens, particularly beyond the kHz range. As the temperature rises, the dispersion region progressively shifts towards higher frequencies. This type of ac conductivity can be explained using Jonscher's power law [25]:

$$\sigma_{ac} = \sigma_{dc} + A\omega^s, \tag{5}$$

where σ_{dc} is the dc conductivity at the plateau region, A and s are temperature-dependent constants where A defines the strength of polarizability, and s indicates the type of conduction mechanisms (e.g., translational hopping motion for $s \leq 1$ and localized hopping for $s \geq 1$) [31]. The s-parameter was calculated from the slope of the frequency-dependent conductivity in the high-frequency region. Fig. 4 (b) shows the variation of the s-parameter with values less than 1. It is observed that the s-parameter decreases with temperature which supported the correlated barrier hopping model [32,33]. This confirms the translational hopping motion involving fast ions in the glass where high mobility ions, such as Na^+, are responsible for the observed electrical conduction and relaxation behavior.

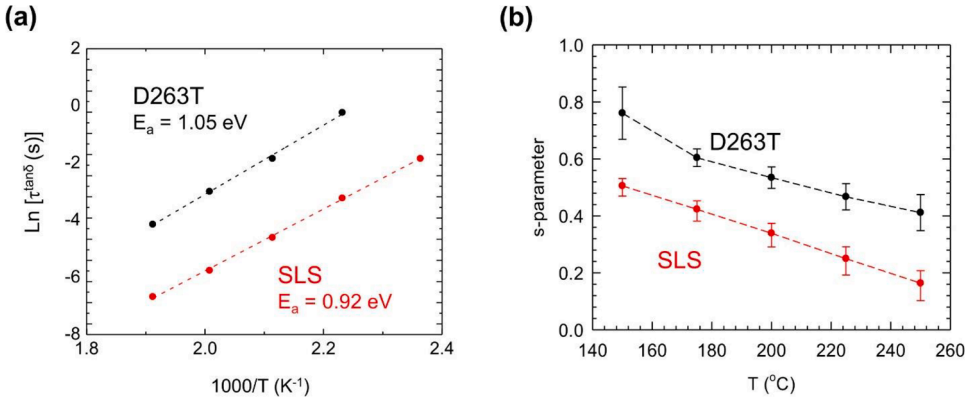

Fig. 4. (a) Temperature-dependent relaxation time and (b) variation of the s-parameter as a function of temperature for SLS and D263T.

3.2. Dielectric displacement and energy loss

Fig. 5 shows the hysteresis loops from dielectric displacement-electric field (D-E) measurements conducted under low-field conditions for SLS and D263T. The hysteresis loops measured at room temperature (RT) are presented in Fig. 5(a-b), while Fig. 5(c-d) shows the hysteresis loops measured at 150 °C. The low-field D-E loops demonstrate a linear response with no significant change in relative permittivity (ε_r) with the applied voltage, which is characteristic of linear dielectric material. However, there is an evident increase in ε_r with increasing temperature. The relative permittivity at RT was calculated from the loop slope, resulting in values of 8.32 for SLS and 6.64 for D263T, which are consistent with values provided by the manufacturer. At 150 °C, both glasses exhibit an increase in ε_r and the loops become wider compared to RT. The obtained ε_r values were found to be 23.30 for SLS and 9.05 for D263T. These values are comparable with the obtained values from the EIS measurements at the same frequency and temperature, with ε_r of 19.84 for SLS and ε_r of 10.51 for D263T.

From the D-E loops in Fig. 5, the amount of energy stored (U_s) and energy discharged (U_d) is calculated by integrating the half-cycle of the dielectric displacement during charging (*from I to II*) and discharging (*from II to III*), respectively. For an ideal capacitor with no dielectric loss, the energy stored, and the discharged energy should be the same. However, for a lossy capacitor, the discharged energy is smaller compared to the energy stored. Thus, the energy efficiency (η) can be estimated as:

$$\eta = \frac{U_d}{U_d + U_l} = \frac{U_d}{U_s}, \tag{6}$$

where U_l is the energy loss which is estimated from the enclosed area under the D-E loop ($U_l = U_s - U_d$). Fig. 6(a-b) shows the variation of U_s, U_d, and η (in %) derived from Fig. 5 for SLS and D263T. The U_s and U_d for SLS and D263T show an increment in value with the electric field and a decrement with increasing temperature. At RT, it is observed that both glasses exhibit an energy efficiency close to 100% which represents the response of an ideal capacitor. However, the energy efficiency decreases with increasing temperature. At 150 °C, the energy efficiency for D263T decreases from 95% to 40%, and in SLS decreases from 90% to 20%. The increment in relative permittivity and decrease in energy efficiency with temperature is attributed to the additional ionic mobility from the thermal energy causing an increase in leakage current and dielectric loss. Since D263T exhibits a higher activation energy for Na^+ migration, a lesser contribution to dielectric loss at the tested conditions is observed.

For comparison, high-field D-E loops, plotted as a half-cycle loop are shown in Fig. 7(a) and (b) for SLS and D263T, respectively. The corresponding parameters (U_s, U_d, and η) are summarized in Table 1. Despite the significant increment in the applied voltage (V = 600 V), the estimated energy efficiency at RT and 150 °C remained consistent with values observed under low-field conditions for both glass samples. This demonstrates linear conduction across the various voltages investigated in this study. It is worth noting that for D263T, the energy efficiency at 10 Hz and 150 °C (η = 8.28%) is lower compared to the 100 Hz (η = 42.86%), as well as lower than SLS at 100 Hz (η = 23.90%). The lower efficiency in D263T is also consistent with the value estimated at low-field conditions under the same frequency and temperature. This is attributed to the higher dielectric loss at 10 Hz compared to 100 Hz, as previously observed in Fig. 3(b).

3.3. Polarization and depolarization currents

During the thermal poling step of the TSDC experiment, the polarization current (I_p) or leakage current was measured for both SLS and D263T, as shown in Fig. 8(a). The measured I_p exhibit two distinctive regions over time. The first region of the current decay at shorter times corresponds to the migration of ionic species. When the poling voltage is applied to the glass sample, mobile ionic species migrate from the anode (or bulk) towards the cathode, resulting in an increased voltage drop

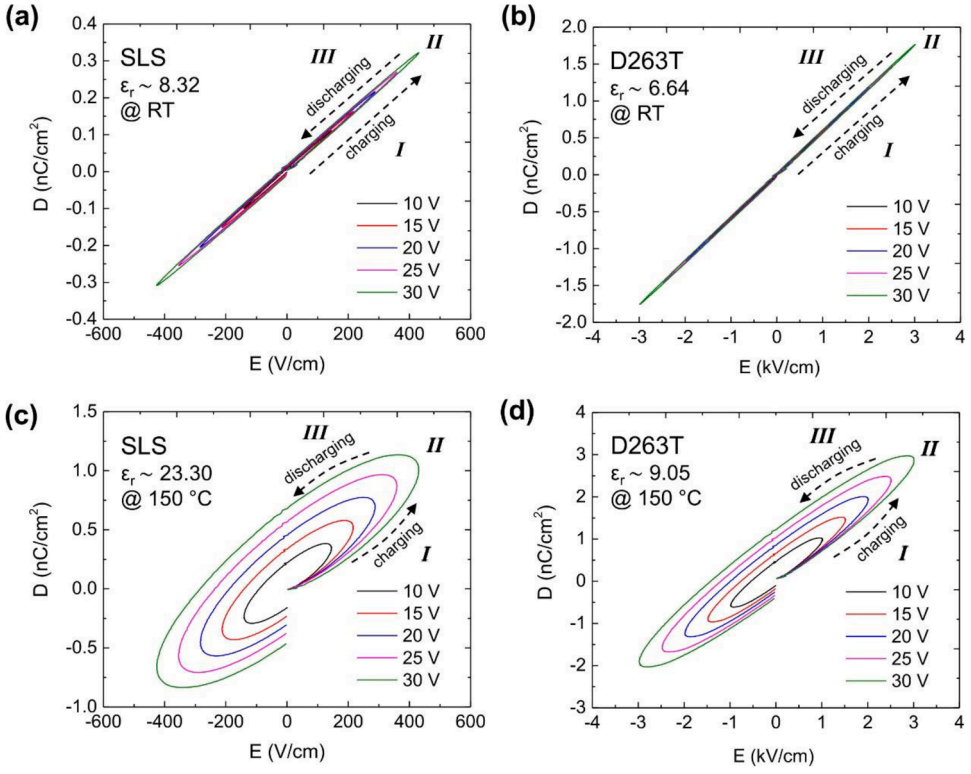

Fig. 5. Low-field D-E loops plotted as full-cycle loops for SLS and D263T glass at (a-b) RT and (c-d) 150 °C measured at different applied voltages with a constant frequency of 100 Hz.

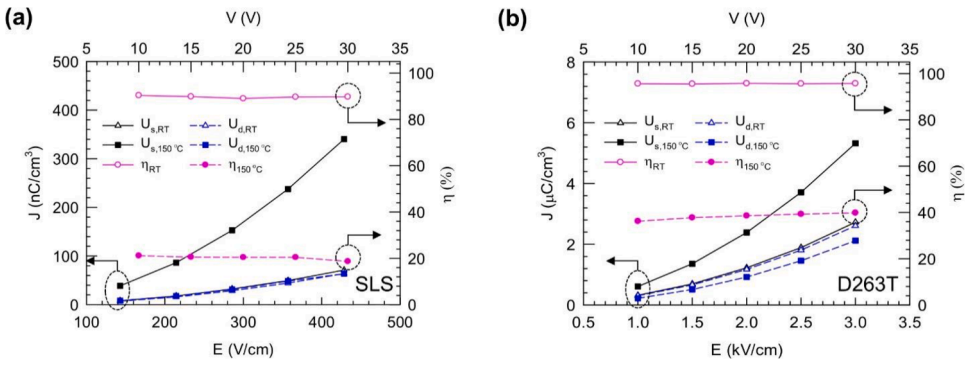

Fig. 6. Energy stored, discharge energy, and energy efficiency at RT and 150 °C for (a) SLS and (b) D263T.

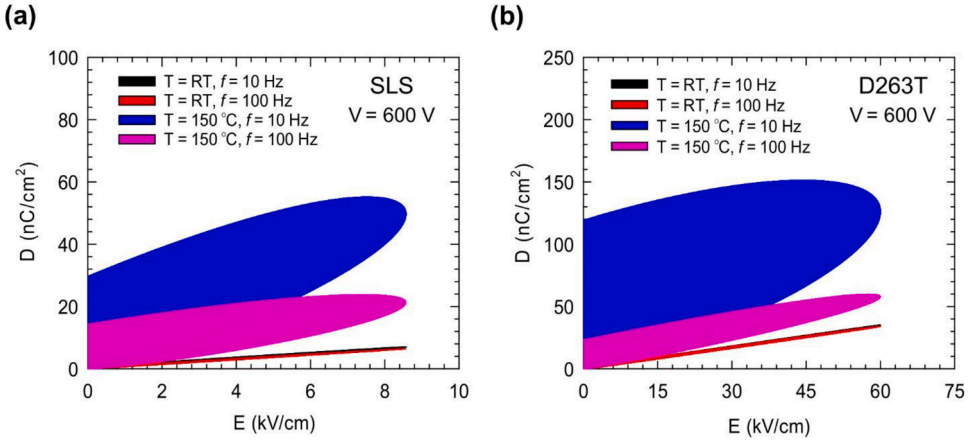

Fig. 7. High-field D-E loops plotted as half-cycle loops for (a) SLS and (b) D263T glass with an applied voltage of 600 V with a constant frequency of 10 Hz and 100 Hz.

Table 1
High-field D-E loop parameters derived from Fig. 7 for SLS and D263T glass.

Sample	Variables		Values			
SLS	Conditions	Applied voltage	600 V			
		Temperature	RT		150 °C	
		Frequency	10 Hz	100 Hz	10 Hz	100 Hz
	Parameters	U_s (mJ/cm^3)	3.13	2.86	32.06	13.87
		U_d (mJ/cm^3)	2.64	2.56	7.66	2.75
		η (%)	84.40	89.67	23.90	19.80
D263T	Conditions	Applied voltage	600 V			
		Temperature	RT		150 °C	
		Frequency	10 Hz	100 Hz	10 Hz	100 Hz
	Parameters	U_s (mJ/cm^3)	107.12	105.47	643.42	213.03
		U_d (mJ/cm^3)	100.53	96.29	53.26	91.31
		η (%)	93.85	91.30	8.28	42.86

Abbreviations: RT = room temperature, U_s = energy stored, U_d = discharge energy, and η = efficiency.

near the anode thus, increasing the electric field in that region. This process can cause significant effects on the structure of the glass, particularly near the anode, as it attempts to compensate for the increased electric field in that region. For instance, it can result in the conversion of NBO to bridging oxygens in SLS and a change in the coordination of boron from B^{IV} to B^{III} in D263T [34]. It is worth noting that other mechanisms for charge compensation, such as proton (H^+) injection, have been previously documented and will be further discussed in the following in this section.

Given the relatively low electric field and temperature employed during the poling step, it is believed that Na^+ ions are the only ions capable of migrating from the anode region and reaching the cathode, hence, the dominant contribution to conduction in both glasses. This assumption is supported by the similarity between the current response between SLS and D263T. The second region of the current decay at longer times is attributed to the formation of a Na-depleted layer at the subsurface of the anode region, along with the accumulation of Na^+ ions at the cathode side [35–38].

Following the first poling condition of 20 V and 250 °C, the intensity of I_p decreases in the short time regime with TSDC cycling (second and third TSDC cycle). This reduction in current can be attributed to multiple factors. One contributing factor is the increase in poling voltage leading

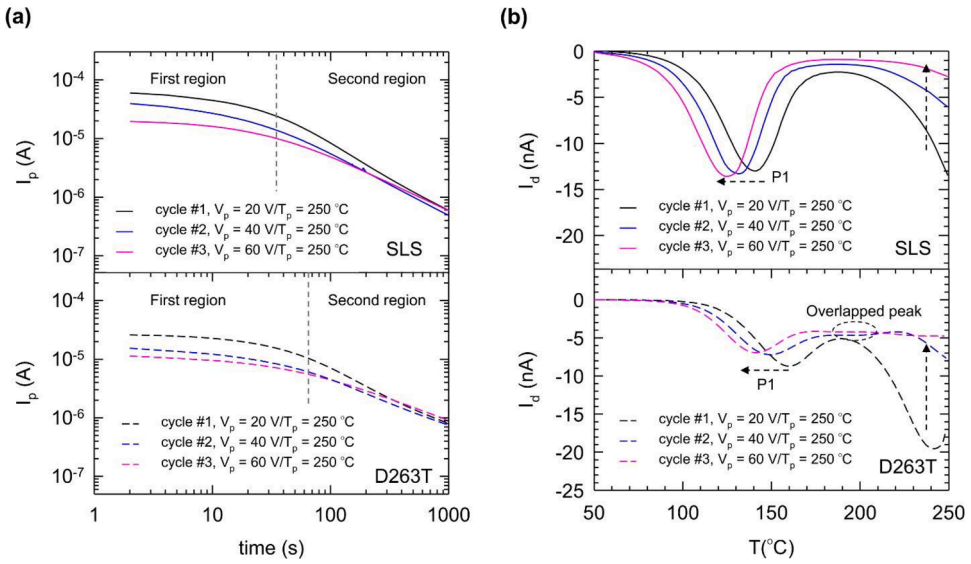

Fig. 8. (a) Polarization current at various poling conditions for SLS and D263T. Both glass samples were poled for 20 mins. Faster current decay in SLS due to the higher Na^+ mobility (b) Corresponding depolarization current measured at a constant heating rate of 10 °C min^{-1}.

to a decrease in the concentration of Na^+ ions near the anode, and the consequent redistribution of the charge carriers within the glass, thus affecting the electric field distribution and current flow. However, since a white precipitate was observed at the cathode surface of both samples, it is possible that a chemical reaction could occur as Na^+ ions reach the cathode. The Na^+ ions can undergo reduction by electrons (e^-) and react with the ambient air (e.g., H_2O, CO_2), leading to a reduction in current. This process can lead to the formation of a white precipitate in the cathode surface, which was observed in both samples. Qiu et al. [39] and An and Fleming [40,41] have also reported this phenomenon in thermally poled SLS and D263T glass sandwiched between two metal contact. Therefore, the findings suggest that the aluminum electrodes evaporated onto the glass samples used in this study do not provide a perfect blocking effect, which is consistent with a previous study using similar electrode configurations [16]. In addition, A. Hein et al. [42] have provided insights into the evolution of blocking characteristics and have risen doubts regarding the assumption that metallized electrodes must always be ion-blocking.

Fig. 8(b) shows the depolarization current of SLS and D263T, respectively, as a function of TSDC cycling. In the first TSDC cycle, both glasses exhibit a distinctive TSDC relaxation peak (P1) at the lowest temperature regime (~ 150 °C), followed by high-temperature background (HTB) above 200 °C. The relaxation process denoted as P1 is attributed to the fast and long-range motion of the Na^+ions moving back towards the anode due to internal residual electric field. The HTB is caused by space-charge effects. The diminishing of the HTB with cycling further supports this hypothesis, as increasing voltage helps in redistributing accumulated charges and reduces the concentration of Na^+ ions through a chemical reaction, as previously suggested. The activation energy for P1 is calculated using the initial rise method [43],

$$I_d = A \cdot \exp\left(-\frac{E_a}{k_b T}\right), \quad (7)$$

where A is a constant, and the other terms were as previously defined. The activation energy values are found to be in the range of 0.73–0.78 eV for SLS and 0.97–1.06 eV for D263T, as shown in Fig. 9. The decrease in activation energy with poling voltage during TSDC cycling supports a hopping-type conduction process. Additionally, these values are in good agreement with the values observed from the EIS measurements confirming Na^+ ions as the dominant ionic specie that contributes to conduction. From the TSDC spectra of the thermally poled D263T, an

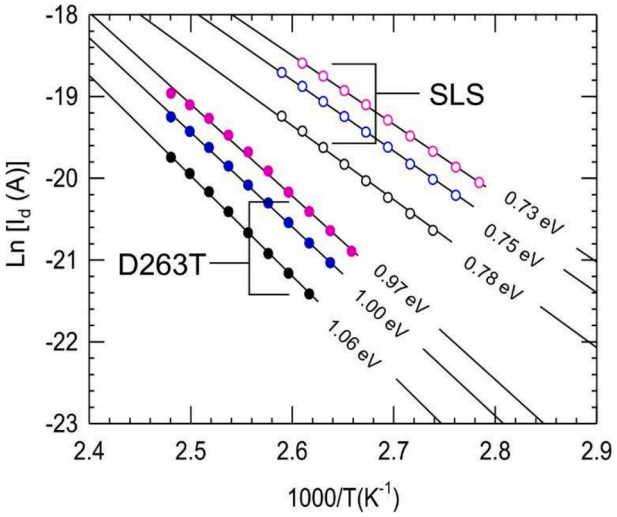

Fig. 9. Linear extrapolation of Eq. (7) to calculate the activation energy responsible for P1 using the slope of the linear fit.

overlapping peak, denoted as the second relaxation peak (P2), is observed around 180–200 °C for the second and third TSDC cycles.

A similar peak in the same temperature range was reported in a previous work by our group for a thermally poled acid-leached SLS, where Na^+ ions from the surfaces were replaced by protonated species and molecular water, creating a more "silica-like" structure. It was suggested that the structural changes and H^+ migration near the anode caused a more limited migration of Na^+ ions during the depolarization process, resulting in the appearance of P2 [16]. Considering that the metallized electrodes used in this study are not perfectly blocking, it is possible for protonated species to be injected from the atmosphere moisture (e.g., H^+ and H_3O^+) or from the dissociation of silanol groups (Si–OH) from the glass surface into the anode as a mean to compensate for the highly intensified electric field in the Na-depleted region [44,45], thereby providing a possible explanation for P2 in D263T, similar to what was observed in the acid-leached SLS glass.

An alternative explanation for P2 is the migration of a second mobile specie in D263T such as K^+ ions. This is supported by the similar activation energy between K^+ and Na^+ ($E_{a,K+}$=1.03 eV ± 0.05 eV [46]).

Previous studies on thermally poled D263T (400 μm in thickness) at 40 V and 140 °C have observed the migration of K^+ ions over a short distance from the anode (< 10 μm) with subsequent accumulation in that region [47]. During depolarization, the movement of K^+ ions back towards the anode is restricted due to their low mobility and larger ionic radius, thus minimizing their contribution to the depolarization current. However, the accumulation of K^+ ions can act as a barrier for Na^+ ions attempting to migrate back, hence causing a more limited or slow migration of Na^+ ions.

4. Conclusion

A comprehensive assessment of the ac and dc characteristics of soda-lime-silica (SLS) and sodium borosilicate (D263T) glasses was conducted using a combination of techniques. EIS measurements provided valuable insights, revealing that the conduction and relaxation phenomena in both glasses are primarily governed by the motion of Na^+ ions. This was supported by the similarity in activation energy estimated from the bulk conductivities and tanδ. The application of Jonscher's power law to describe the ac conductivity variation indicated that Na^+ transport occurs through a hopping mechanism, as evidenced by the s-parameters being less than 1 for both glasses. The D-E hysteresis loops exhibited a linear conduction response at low and high fields, with the energy efficiency primarily influenced by the Na^+ content and mobility. Consequently, D263T exhibited a less detrimental energy loss compared to SLS. TSDC analysis revealed a distinctive relaxation peak (P1) associated with the fast and long-range hopping motion of Na^+ ions in both glasses. The calculated activation energy values obtained from TSDC experiments aligned well with those from EIS measurements, with SLS exhibiting a lower activation energy compared to D263T.In the case of D263T, a second relaxation peak (P2) was observed during TSDC analysis. It is hypothesized that P2 arises from the short-range migration and accumulation of a second mobile species near the anode, acting as a barrier and limiting Na^+ ions to migrate back during the depolarization process.

CRediT authorship contribution statement

Cesar A. Nieves: Investigation, Methodology, Formal analysis, Visualization, Writing – original draft, Writing – review & editing. **Michael T. Lanagan:** Supervision, Conceptualization, Methodology, Funding acquisition, Writing – review & editing.

Declaration of Competing Interest

The authors declare that they have no known competing financial interests or personal relationships that could have appeared to influence the work reported in this paper.

Data availability

Data will be made available on request.

Acknowledgments

This material is based on work supported by the National Science Foundation (NSF) Graduate Research Fellowship Program (DGE1255832) and the NSF-INTERN program through the Center for Dielectrics and Piezoelectrics under Grant IIP-1841453 and Grant IIP-1841466. Any opinions, findings, conclusions, or recommendations expressed in this material are those of the authors and do not necessarily reflect the views of the National Science Foundation. The authors would like to thank Steven Perini and Jeff Long from The Material Characterization Laboratory at Penn State for their technical support during measurements and to Prof. Seong H. Kim, Professor of Chemistry Engineering at Penn State for providing glass samples.

References

[1] D.L. Morse, J.W. Evenson, Welcome to the glass age, Int. J. Appl. Glass Sci. 7 (4) (2016) 409–412, https://doi.org/10.1111/ijag.12242.
[2] A.K. Varshneya, J.C. Mauro, Fundamentals of Inorganic Glasses, Elsevier, 2019.
[3] F.M.E. Eldin, N.A. El Alaily, Electrical conductivity of some alkali silicate glasses, Mater. Chem. Phys. 52 (2) (1998) 175–179, https://doi.org/10.1016/S0254-0584(98)80021-7. Feb.
[4] M.T. Lanagan, L. Cai, L.A. Lamberson, J. Wu, E. Streltsova, N.J. Smith, Dielectric polarizability of alkali and alkaline-earth modified silicate glasses at microwave frequency, Appl. Phys. Lett. 116 (22) (2020), 222902, https://doi.org/10.1063/5.0008646. Jun.
[5] C. Huang, A.N. Cormack, The structure of sodium silicate glass, J. Chem. Phys. 93 (11) (1990) 8180–8186, https://doi.org/10.1063/1.459296. Dec.
[6] Y. Yu, B. Stevensson, M. Edén, Structural role of sodium in borosilicate, phosphosilicate, and borophosphosilicate glasses unveiled by solid-state NMR and MD simulations, J. Phys. Chem. C 123 (42) (2019) 25816–25832, https://doi.org/10.1021/acs.jpcc.9b06823. Oct.
[7] P. Lv, C. Wang, B. Stevensson, Y. Yu, T. Wang, M. Edén, Impact of the cation field strength on physical properties and structures of alkali and alkaline-earth borosilicate glasses, Ceram. Int. 48 (13) (2022) 18094–18107, https://doi.org/10.1016/j.ceramint.2022.03.022. Jul.
[8] A.C. Wright, "Borate structures: crystalline and vitreous," Physics and Chemistry of Glasses - European Journal of Glass Science and Technology Part B, vol. 51, no. 1, pp. 1–39, Feb. 2010.
[9] L.A. Nevolina, O.N. Koroleva, N.G. Tyurnina, Z.G. Tyurnina, Study of alkaline earth borosilicate glass by raman spectroscopy, Glass Phys. Chem 47 (1) (2021) 24–29, https://doi.org/10.1134/S1087659621010090. Jan.
[10] M.S. Bødker, S.S. Sørensen, J.C. Mauro, M.M. Smedskjaer, Predicting composition-structure relations in alkali borosilicate glasses using statistical mechanics, Front. Mater. 6 (2019), https://doi.org/10.3389/fmats.2019.00175.
[11] C.C. Hunter, M.D. Ingram, Na+-ion conducting glasses, Solid State Ionics 14 (1) (1984) 31–40, https://doi.org/10.1016/0167-2738(84)90007-9. Sep.
[12] D. Ravaine, Ionic transport properties in glasses, J. Non Cryst. Solids 73 (1) (1985) 287–303, https://doi.org/10.1016/0022-3093(85)90355-2. Aug.
[13] C.H. Hsieh, H. Jain, E.I. Kamitsos, Correlation between dielectric constant and chemical structure of sodium silicate glasses, J. Appl. Phys. 80 (3) (1996) 1704–1712, https://doi.org/10.1063/1.363824. Aug.
[14] W. Luo, et al., Potential-induced degradation in photovoltaic modules: a critical review, Energy Environ. Sci. 10 (1) (2017) 43–68, https://doi.org/10.1039/C6EE02271E. Jan.
[15] V. Naumann, D. Lausch, and C. Hagendorf, "Sodium Decoration of PID-s Crystal Defects after Corona Induced Degradation of Bare Silicon Solar Cells," Energy Procedia, vol. 77, pp. 397–401, Aug. 2015, doi: 10.1016/j.egypro.2015.07.055.
[16] C.A. Nieves, A.L. Ogrinc, E. Furman, K.H. Seong, M.T. Lanagan, Ion migration study in acid-leached soda–lime–silica glass by thermally stimulated depolarization current analysis, J. Am. Ceram. Soc. (2023) 1–13, https://doi.org/10.1111/jace.19064.
[17] E. Thienot, F. Domingo, E. Cambril, C. Gosse, Reactive ion etching of glass for biochip applications: composition effects and surface damages, Microelectron. Eng. 83 (2006) 1155–1158, https://doi.org/10.1016/j.mee.2006.01.029.
[18] A.K. Agarwal, D.E. Day, Thermally stimulated currents and alkali-ion motion in silicate glasses, J. Am. Ceram. Soc. 65 (2) (1982) 111–117, https://doi.org/10.1111/j.1151-2916.1982.tb10367.x.
[19] B. Dutta, D.E. Day, Electronic and ionic conduction in sodium borosilicate glasses, J. Non Cryst. Solids 48 (2) (1982) 345–357, https://doi.org/10.1016/0022-3093(82)90170-3. Apr.
[20] C.M. Hong, D.E. Day, Thermally stimulated polarization and depolarization current (TSPC/TSDC) techniques for studying ion motion in glass, J. Mater. Sci. 14 (10) (1979) 2493–2499, https://doi.org/10.1007/BF00737040. Oct.
[21] A.H. Bhuiyan, S. Ahmed, Thermally stimulated depolarisation current in sodium-potassium borosilicate glass, J. Non Cryst. Solids 43 (3) (1981) 353–363, https://doi.org/10.1016/0022-3093(81)90103-4. Apr.
[22] H.D. Jannek, D.E. Day, Sodium motion in phase-separated sodium silicate glasses, J. Am. Ceram. Soc. 64 (4) (1981) 227–233, https://doi.org/10.1111/j.1151-2916.1981.tb10274.x.
[23] J.O. Isard, The mixed alkali effect in glass, J. Non Cryst. Solids 1 (3) (1969) 235–261, https://doi.org/10.1016/0022-3093(69)90003-9.
[24] B. Roling, M.D. Ingram, Mixed alkaline–earth effects in ion conducting glasses, J. Non Cryst. Solids 265 (1) (2000) 113–119, https://doi.org/10.1016/S0022-3093(99)00899-6. Mar.
[25] A.K. Jonscher, Dielectric relaxation in solids, J. Phys. D Appl. Phys. 32 (14) (1999) R57, https://doi.org/10.1088/0022-3727/32/14/201. Jul.
[26] J.B. Jorcin, M.E. Orazem, N. Pébère, B. Tribollet, CPE analysis by local electrochemical impedance spectroscopy, Electrochim. Acta 51 (8) (2006) 1473–1479, https://doi.org/10.1016/j.electacta.2005.02.128. Jan.
[27] C.R. Mariappan, B. Roling, Mechanism and kinetics of Na+ ion depletion under the anode during electro-thermal poling of a bioactive glass, J. Non Cryst. Solids 356 (11) (2010) 720–724, https://doi.org/10.1016/j.jnoncrysol.2009.03.013. Apr.
[28] D.E. Carlson, K.W. Hang, G.F. Stockdale, Electrode 'polarization' in alkali-containing glasses, J. Am. Ceram. Soc. 55 (7) (1972) 337–341, https://doi.org/10.1111/j.1151-2916.1972.tb11305.x.

[29] D.E. Carlson, Ion depletion of glass at a blocking anode: I, theory and experimental results for alkali silicate glasses, J. Am. Ceram. Soc. 57 (7) (1974) 291–294, https://doi.org/10.1111/j.1151-2916.1974.tb10903.x.
[30] E.C. Ziemath, C.A. Escanhoela, M.L. Braunger, Comparison of activation energies for the electrical conductivity of silicate glasses obtained by dc and ac techniques, Solid State Ionics 301 (2017) 146–151, https://doi.org/10.1016/j.ssi.2017.01.025. Mar.
[31] K. Funke, Jump relaxation in solid ionic conductors, Solid State Ionics 28–30 (1988) 100–107, https://doi.org/10.1016/S0167-2738(88)80015-8. Sep.
[32] A. Ghosh, Transport properties of vanadium germanate glassy semiconductors, Phys. Rev. B 42 (9) (1990) 5665–5676, https://doi.org/10.1103/PhysRevB.42.5665. Sep.
[33] M. Dult, R.S. Kundu, S. Murugavel, R. Punia, N. Kishore, Conduction mechanism in bismuth silicate glasses containing titanium, Physica B 452 (2014) 102–107, https://doi.org/10.1016/j.physb.2014.07.004.
[34] A. Tandia, M. Reveil, K.D. Vargheese, J. Luo, J.C. Mauro, P. Clancy, Modeling the thermal poling of glasses using molecular dynamics. Part 1: effects on glass structure, J. Non Cryst. Solids 461 (2017) 98–103, https://doi.org/10.1016/j.jnoncrysol.2017.01.045. Apr.
[35] D.L. Kinser, L.L. Hench, Electrode polarization in alkali silicate glasses, J. Am. Ceram. Soc. 52 (12) (1969) 638–641, https://doi.org/10.1111/j.1151-2916.1969.tb16066.x.
[36] P.M. Sutton, Space charge and electrode polarization in glass, II, J. Am. Ceram. Soc. 47 (5) (1964) 219–230, https://doi.org/10.1111/j.1151-2916.1964.tb14400.x.
[37] T.M. Proctor, P.M. Sutton, Space-charge development in glass, J. Am. Ceram. Soc. 43 (4) (1960) 173–178, https://doi.org/10.1111/j.1151-2916.1960.tb12977.x.
[38] K.J. Keller, Formation and annulment of space charges glass and their influence on electric breakdown, Phys. Rev. 86 (5) (1952) 804–805, https://doi.org/10.1103/PhysRev.86.804. Jun.
[39] M. Qiu, F. Pi, G. Orriols, M. Bibiche, Signal damping of second-harmonic generation in poled soda-lime silicate glass, JOSA B 15 (4) (1998) 1362–1365, https://doi.org/10.1364/JOSAB.15.001362. Apr.
[40] H. An, S. Fleming, Second-order optical nonlinearity in thermally poled borosilicate glass, Appl. Phys. Lett. 89 (18) (2006), 181111, https://doi.org/10.1063/1.2374690. Oct.
[41] H. An, S. Fleming, Second-order optical nonlinearity and accompanying near-surface structural modifications in thermally poled soda-lime silicate glasses, JOSA B 23 (11) (2006) 2303–2309, https://doi.org/10.1364/JOSAB.23.002303. Nov.
[42] A. Hein, M. Schäfer, K.M. Weitzel, Electron attachment induced ion transport– Part II: the evolution of blocking of charge transport, Solid State Ionics 339 (15) (2019), 114997, https://doi.org/10.1016/j.ssi.2019.06.005.
[43] J.van. Turnhout, Thermally stimulated discharge of polymer electrets, Polym. J. 2 (2) (1971) 173–191, https://doi.org/10.1295/polymj.2.173.
[44] D.E. Carlson, Anodic proton injection in glasses, J. Am. Ceram. Soc. 57 (11) (1974) 461–466, https://doi.org/10.1111/j.1151-2916.1974.tb11390.x.
[45] N.J. Smith, C.G. Pantano, Structural and compositional modification of a barium boroaluminosilicate glass surface by thermal poling, Appl. Phys. A 116 (2014) 529–543, https://doi.org/10.1007/s00339-014-8467-3.
[46] A. Hein, M. Schäfer, K.M. Weitzel, Electron attachment induced ion transport — Part I: conductivities and activation energies, Solid State Ionics 339 (15) (2019), 114996, https://doi.org/10.1016/j.ssi.2019.06.004.
[47] K. Rein, M. Schäfer, K.M. Weitzel, The role of dielectric breakdown in the electro-thermal poling of D263T glass, IEEE Trans. Dielectr. Electr. Insul. 27 (5) (2020) 1422–1427, https://doi.org/10.1109/TDEI.2020.008814. Oct.